

Autocorrelation-based convolutional neural network for reconstruction of noisy attosecond streaking traces

Xiaoxian Zhu(朱孝先), Yitan Gao(高亦谈), Yiming Wang(王一鸣), Kun Zhao(赵昆), and Zhiyi Wei(魏志义)
Citation: Chin. Phys. B, 2026, 35 (**5**): 054204. DOI: 10.1088/1674-1056/ae3474
http://cpb.iphy.ac.cn; http://iopscience.iop.org/cpb

What follows is a list of articles you may be interested in

Full stabilization of eight-channel Yb-fiber coherent beam combining system delivering 1.18-kW, 1.18-mJ, 270-fs pulses

Zhuo Shi(史卓), Zhi-Hang Du(杜志航), Cheng-Bin Liang(梁成斌), Hong-Xiang Chang(常洪祥), Zi-Kai Dong(董自凯), Hong-Yu Guo(郭鸿宇), Can Li(李灿), Pu Zhou(周朴), Zhi-Yi Wei(魏志义), and Guo-Qing Chang(常国庆)
Chin. Phys. B, 2026, 35 (**2**): 024210. DOI: 10.1088/1674-1056/ae1952

3D-GTDSE: A GPU-based code for solving 3D-TDSE in Cartesian coordinates

Ke Peng(彭科), Aihua Liu(刘爱华), Jun Wang(王俊), and Xi Zhao(赵曦)
Chin. Phys. B, 2025, 34 (**9**): 094203. DOI: 10.1088/1674-1056/adee00

Effect of pulse duration on generation of attosecond pulse with coherent wake emission

Siyu Chen(陈思宇), Zhinan Zeng(曾志男), and Ruxin Li(李儒新)
Chin. Phys. B, 2021, 30 (**11**): 114206. DOI: 10.1088/1674-1056/abf4be

Effects of initial electronic state on vortex patterns in counter-rotating circularly polarized attosecond pulses

Qi Zhen(甄琪), Jia-He Chen(陈佳贺), Si-Qi Zhang(张思琪), Zhi-Jie Yang(杨志杰), and Xue-Shen Liu(刘学深)
Chin. Phys. B, 2021, 30 (**2**): 024203. DOI: 10.1088/1674-1056/abb7fb

Role of quantum paths in generation of attosecond pulses

M R Sami and A Shahbaz†
Chin. Phys. B, 2020, 29 (**10**): 104207. DOI: 10.1088/1674-1056/ab9deb

Photoelectron momentum distributions of single-photon ionization under a pair of elliptically polarized attosecond laser pulses

Hui-Fang Cui(崔会芳), Xiang-Yang Miao(苗向阳)
Chin. Phys. B, 2020, 29 (**7**): 074203. DOI: 10.1088/1674-1056/ab8ac0

Autocorrelation-based convolutional neural network for reconstruction of noisy attosecond streaking traces

Xiaoxian Zhu(朱孝先)[1,2], Yitan Gao(高亦谈)[1,2], Yiming Wang(王一鸣)[2], Kun Zhao(赵昆)[1,2,†], and Zhiyi Wei(魏志义)[1,2]

[1] *Songshan Lake Materials Laboratory, Dongguan* 523808, *China*
[2] *Beijing National Laboratory for Condensed Matter Physics, Institute of Physics, Chinese Academy of Sciences, Beijing* 100190, *China*

(Received 3 December 2025; revised manuscript received 24 December 2025; accepted manuscript online 7 January 2026)

Attosecond light sources serve as crucial tools for investigating the ultrafast electronic dynamics in matter with remarkable temporal resolution. Traditional methods face difficulties in accurately measuring attosecond pulses, and the prevailing approach involves utilizing attosecond streak cameras coupled with inversion algorithms to reconstruct phase information. However, these algorithms often require multiple iterations and extensive computational time. This study investigates the utilization of autocorrelation graphs as inputs for a convolutional neural network (CNN) to invert streaking traces obtained by attosecond streak camera. We explore the noise resistance capability of autocorrelation within the CNN inversion and aim to provide a physical explanation for its effectiveness. The objective of this research is to enhance the accuracy and reliability of CNN inversion for attosecond streaking traces, enabling improved resilience against experimental noises.

Keywords: attosecond, convolutional neural networks, autocorrelation, attosecond streaking camera, phase retrieval, noise robustness

PACS: 42.65.Re, 42.30.–d, 42.50.Hz, 07.05.Mh

DOI: 10.1088/1674-1056/ae3474 **CSTR:** 32038.14.CPB.ae3474

Attosecond light sources provide access to ultrafast electron dynamics with unprecedented temporal resolution, enabling real-time observation and control of electronic motion, with a broad range of applications in physics, chemistry, and biomedicine.[1–6] Since the first successful generation of an isolated 650-attosecond pulse in 2001,[7] researchers have continuously pursued shorter pulse durations, with the current record reaching 43 as reported in Ref. [8]. Despite these achievements, accurate measurement of attosecond pulses remains a major challenge, largely due to their high photon energy and limited photon number. The attosecond streak camera is the mainstream tool for pulse characterization. In this technique, photoelectron wave packets ionized by attosecond pulses are accelerated by an infrared (IR) laser field, and the streaked photoelectron spectra at different pump–probe delays are measured. The spectral phase of the attosecond pulse is then retrieved through inversion algorithms. Representative methods include frequency-resolved optical gating for complete reconstruction of attosecond bursts (FROG-CRAB),[9–11] phase retrieval by omega oscillation filtering (PROOF),[12] the extended ptychographic iterative engine (ePIE),[13] the Volkov transform generalized projection algorithm (VTGPA),[14] and genetic-algorithm-based methods such as PROBP.[15] However, these algorithms generally require multiple iterations and long computation time, limiting their efficiency in practice.

Machine learning, particularly deep learning, has shown great potential for solving complex nonlinear problems in data and image analysis.[16–18] Convolutional neural networks (CNNs) can extract hierarchical features from images and establish mapping relations between input and output data. Previous studies have applied CNNs to attosecond streaking inversion.[19–21] Nevertheless, existing CNN approaches face two critical issues: (i) the training processes are purely data-driven and lack physical interpretability, and (ii) they depend on noise-free synthetic datasets, while real experimental data are inevitably corrupted by noise.

We implement a convolutional neural network for phase retrieval in attosecond streaking measurements using the TensorFlow package[22] with GPU acceleration. As a supervised learning algorithm, the CNN is trained to map input images to a probability distribution over labels. The model's performance is fundamentally limited by the quality and quantity of the training data.

In attosecond streaking measurements, electrons are ionized by attosecond pulses and subsequently accelerated in the continuum under the influence of an IR laser field. This physical process is governed by the time-dependent Schrödinger equation:[23]

$$\mathrm{i}\partial_t \Psi(\boldsymbol{r}) = \left[-\frac{1}{2}\nabla^2 - \frac{1}{r} - \boldsymbol{r}\cdot\boldsymbol{E}(t)\right]\Psi(\boldsymbol{r}), \tag{1}$$

†Corresponding author. E-mail: zhaokun@iphy.ac.cn

© 2026 Chinese Physical Society and IOP Publishing Ltd. All rights, including for text and data mining, AI training, and similar technologies, are reserved.

where $\boldsymbol{E}(t) = \boldsymbol{E}_l(t) + \boldsymbol{E}_x(t)$ comprises both the laser field $\boldsymbol{E}_l(t)$ and the attosecond pulse electric field $\boldsymbol{E}_x(t)$.

Within the strong-field approximation framework, we neglect all intermediate excited states and assume direct ionization from the ground state to the continuum.[24] Furthermore, the Coulomb potential is disregarded due to its relative weakness compared to the laser field. This yields the forward calculation formula for electron spectra from attosecond pulses:[25]

$$\begin{aligned} I(\boldsymbol{p},\tau) &= \left| \int_{-\infty}^{+\infty} \boldsymbol{E}_x(t)\, \mathrm{d}[\boldsymbol{p}+\boldsymbol{A}(t+\tau)] \exp[\mathrm{i}\phi(\boldsymbol{p},t+\tau)] \right. \\ &\quad \left. \times \exp\left[-\mathrm{i}\left(\frac{1}{2}\boldsymbol{p}^2 + I_\mathrm{p}\right)t\right] \mathrm{d}t \right|^2, \\ \phi(\boldsymbol{p},t+\tau) &= -\int_{t+\tau}^{+\infty} \left[\boldsymbol{p}\cdot\boldsymbol{A}(t') + \frac{1}{2}\boldsymbol{A}^2(t')\right] \mathrm{d}t', \end{aligned} \tag{2}$$

Here $\boldsymbol{A}(t)$ represents the vector potential of the IR laser. The term $\boldsymbol{E}_x(t)\,\mathrm{d}[\boldsymbol{p}+\boldsymbol{A}(t+\tau)]$ corresponds to the photoelectron wave packet ionized by the attosecond pulse, with $\mathrm{d}[\boldsymbol{p}+\boldsymbol{A}(t+\tau)]$ denoting the transition matrix element between the ground and continuum states. The phase modulation $\exp[\mathrm{i}\phi(\boldsymbol{p},t+\tau)]$ accounts for the laser-induced phase accumulation, while τ indicates the delay between attosecond and laser pulses. The measured streaking trace intensity $I(\boldsymbol{p},\tau)$ is thus obtained.

Assuming the femtosecond IR pulse characteristics are known and the attosecond pulse spectrum is experimentally determined, the spectral phase in the frequency domain is expanded as

$$\varphi(\Omega) = a_2\frac{(\Omega-\Omega_0)^2}{(\Delta\Omega/2)^2} + a_3\frac{(\Omega-\Omega_0)^3}{(\Delta\Omega/2)^3} + a_4\frac{(\Omega-\Omega_0)^4}{(\Delta\Omega/2)^4}, \tag{3}$$

where a_2, a_3, and a_4 represent the second, third, and fourth-order dispersion coefficients to be retrieved, Ω_0 is the central photon energy, and $\Delta\Omega$ denotes the full width at half maximum of the spectrum. Since the zeroth and first-order phase terms do not affect the pulse duration and introduce retrieval ambiguities, they are set to zero to ensure unique solutions, focusing exclusively on higher-order dispersion effects. Once both the spectral phase $\phi(\Omega)$ and the spectrum $I(\Omega)$are obtained, the attosecond pulse in the frequency domain can be expressed as $E_\mathrm{XUV}(\Omega) = \sqrt{I(\Omega)}\,\mathrm{e}^{\mathrm{i}\phi(\Omega)}$.

The streaking traces calculated by this model, which directly integrates the strong-field approximation formulas rather than employing the central momentum approximation, provide more rigorous physical constraints than conventional FROG-CRAB methods.[9] Here, the dispersion coefficients serve as ground-truth labels for validating CNN predictions, while the corresponding streaking traces constitute the training data input to the network.

Given the CNN's sensitivity to image features and the localized nature of dispersion-induced modifications in attosecond streaking traces (primarily near the central energy region), direct utilization of raw streaking traces as CNN inputs proves imperfect. The relevant features occupy only a small fraction of the image, hindering effective feature extraction and computational efficiency. To amplify the characteristic signatures of dispersion effects, we convert streaking traces into autocorrelation maps through correlation coefficient analysis.[15,26] For a given streaking trace $S(E,\tau)$, the correlation coefficient that quantifies the signal similarity between two time delays, $S_\alpha = S(E_{1,2,3,\ldots,N},\tau_\alpha)$ and $S_\beta = S(E_{1,2,3,\ldots,N},\tau_\beta)$, is defined as

$$C_{\alpha\beta} = \frac{\sum_{i=1}^{N}\left[S(E_i,\tau_\alpha)-\overline{S}_\alpha\right]\left[S(E_i,\tau_\beta)-\overline{S}_\beta\right]}{\sqrt{\sum_{i=1}^{N}\left[S(E_i,\tau_\alpha)-\overline{S}_\alpha\right]^2}\sqrt{\sum_{i=1}^{N}\left[S(E_i,\tau_\beta)-\overline{S}_\beta\right]^2}}, \tag{4}$$

where the mean values of the signals are

$$\overline{S}_\alpha = \frac{1}{N}\sum_{i=1}^{N} S(E_i,\tau_\alpha), \quad \overline{S}_\beta = \frac{1}{N}\sum_{i=1}^{N} S(E_i,\tau_\beta),$$

corresponding to the signals S_α and S_β, respectively.

The correlation coefficient ranges from -1 (perfect anti-correlation) to 1 (perfect correlation), with zero indicating no correlation. For streaking traces comprising M delay steps, this generates $M\times M$ autocorrelation coefficient maps that exhibit distinct patterns for different dispersion parameters, as illustrated in Fig. 1.

To enhance experimental relevance, we incorporate Poisson noise into simulated training data, mimicking statistical fluctuations inherent in electron counting detection. The Poisson noise

$$S = \mathrm{Poisson}\left(\lambda_\mathrm{p} S_0\right) \tag{5}$$

perturbs the normalized theoretical trace S_0, where λ_p controls the noise level corresponding to average electron counts per detection channel. Lower λ_p values indicate higher relative noise, realistically simulating finite-electron statistics and detector quantum efficiency limitations. This noise inclusion in the training data improves CNN robustness when processing experimental data with low-count signals.

Our training dataset comprises 10^5 simulated streaking traces with randomly generated dispersion coefficients and IR pulse durations, converted to autocorrelation maps via Eq. (4). To ensure diversity, we employ both Gaussian and hyperbolic secant profiles for attosecond spectra and IR envelopes. An additional 2×10^4 traces form the validation set. All traces undergo Poisson noise injection with λ_p ranging from 100 to 1000, simulating the conditions of experimental data as close as possible.

The loss function plays a critical role in quantifying the discrepancy between model predictions and actual observations, facilitating model training and optimization, enabling performance evaluation, regularizing against overfitting, and

guiding model selection and hyperparameter tuning. In this work, we define a physically guided loss function as

$$L_\varphi = \frac{1}{n}\sum_{i=1}^{n}\left[\left(y_{\text{true}}[i] - y_{\text{pred}}[i]\right)^2 \times I_{\text{true}}[i]\right], \tag{6}$$

where y_{true} denotes the true spectral phase, y_{pred} represents the CNN-predicted phase, and I_{true} is the measured spectrum. In spectral phase retrieval, the contribution of phase errors at different frequencies to the resulting temporal pulse profile varies significantly. To enhance the energy-resolved accuracy of phase predictions, we introduce the spectral intensity as a scaling factor in the loss function, effectively weighting the phase prediction errors according to their physical impact on the temporal waveform. This approach imposes a physically motivated constraint that directs the CNN's attention to phase components that predominantly influence the temporal pulse structure, thereby improving prediction fidelity by aligning the learning process with the underlying physics.

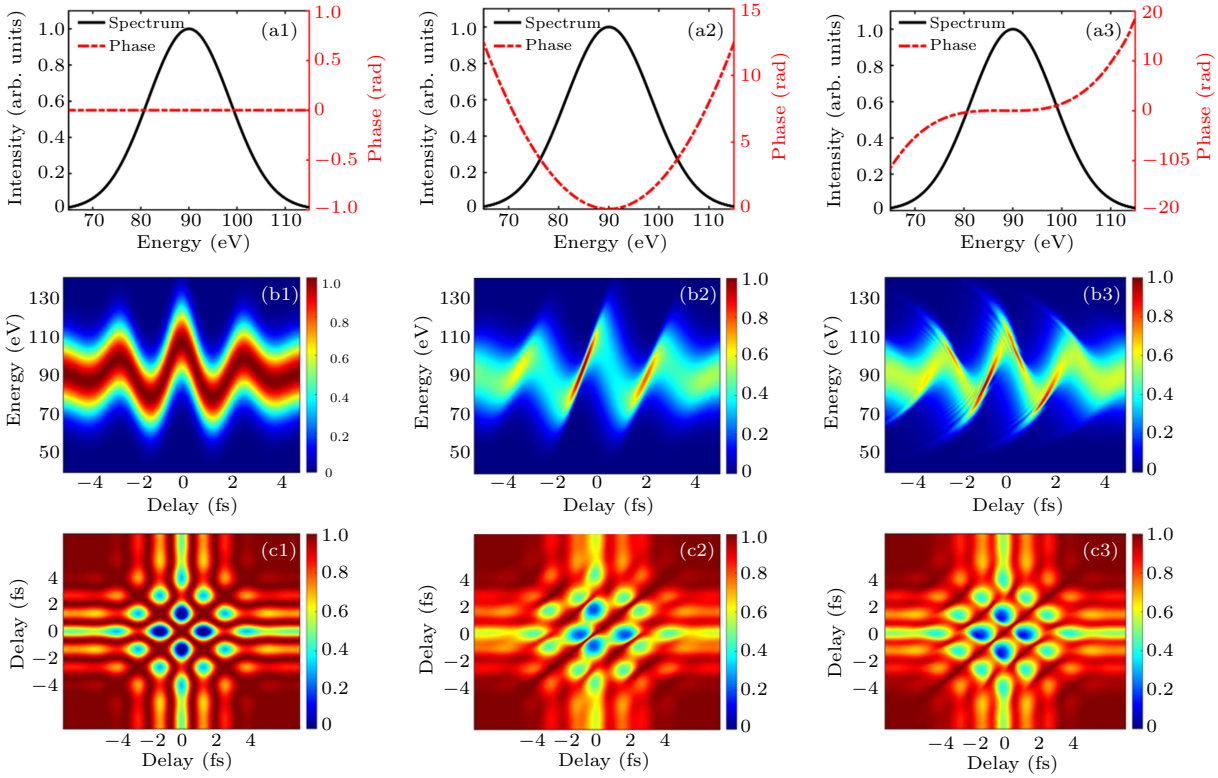


Fig. 1. Streaking traces and autocorrelations of attosecond pulses. (a1)–(a3) Spectra and phases used to generate the corresponding streaking traces and autocorrelations. (b1)–(b3) Streaking traces of the attosecond pulses. (c1)–(c3) Autocorrelation traces of the attosecond pulses.

The implemented CNN architecture comprises four convolutional layers, each consisting of convolution, nonlinear activation, and pooling operations, followed by four fully connected layers that ultimately output the spectral phase. The Adam optimizer[27] is employed during training, with validation performed after each epoch to monitor for overfitting and to assess model performance for subsequent refinement. A schematic of the complete network structure is presented in Fig. 2.

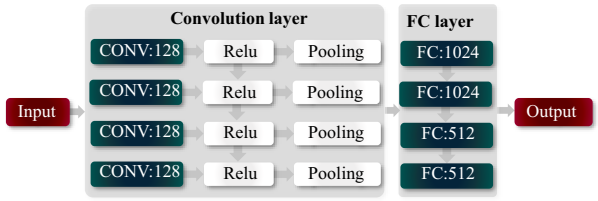


Fig. 2. Schematic diagram of the CNN architecture used in this study.

Based on the generated training data, we train two distinct convolutional neural network models to map either a streaking trace or an autocorrelation trace to the spectral phase of an attosecond pulse. The models are first trained and validated using separate datasets. After convergence, an independent test set of 20 samples is fed into the trained models to predict the spectral phase.

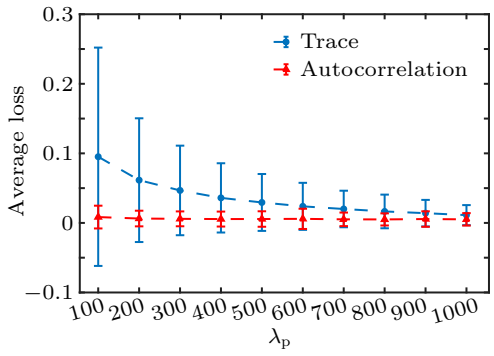


Fig. 3. Mean loss of the test set under different noise levels. Error bars indicate the standard deviation of the loss over 20 test samples.

To evaluate the noise robustness of both models, we compute the loss function, defined by Eq. (6), for each of the 20 test

inputs under varying noise levels. The mean loss over the test set is used as a performance metric. As shown in Fig. 3, the mean loss of the streaking-based model is significantly higher than that of the autocorrelation-based model. Moreover, as the noise level decreases (i.e., with increasing λ_p), the mean loss of the streaking model decreases, whereas the autocorrelation model remains largely unaffected. This indicates that the autocorrelation model exhibits superior robustness against input noise.

We further visualize the phase retrieval results under different noise levels ($\lambda_p = 1000$, 500, 100, 50), as summarized in Fig. 4. In the low-noise regime (e.g., $\lambda_p = 1000$), both models yield predictions in close agreement with the ground truth [Figs. 4(c1) and 4(d1)]. However, as noise increases, the streaking model degrades significantly, while the autocorrelation model maintains accurate predictions across all noise levels. This underscores the advantage of using autocorrelation traces in noisy environments.

We attribute this robustness to two factors. First, the autocorrelation computation involves averaging over spectral intensities at different delays, which inherently suppresses random noise. Second, phase-induced spectral oscillations are amplified in the autocorrelation representation. As illustrated in Fig. 1, such oscillations are localized near central energies in streaking traces but are more globally distributed in autocorrelation traces. Since CNNs rely on discriminative features in input images, the autocorrelation representation provides stronger and more noise-resistant signatures for phase retrieval.

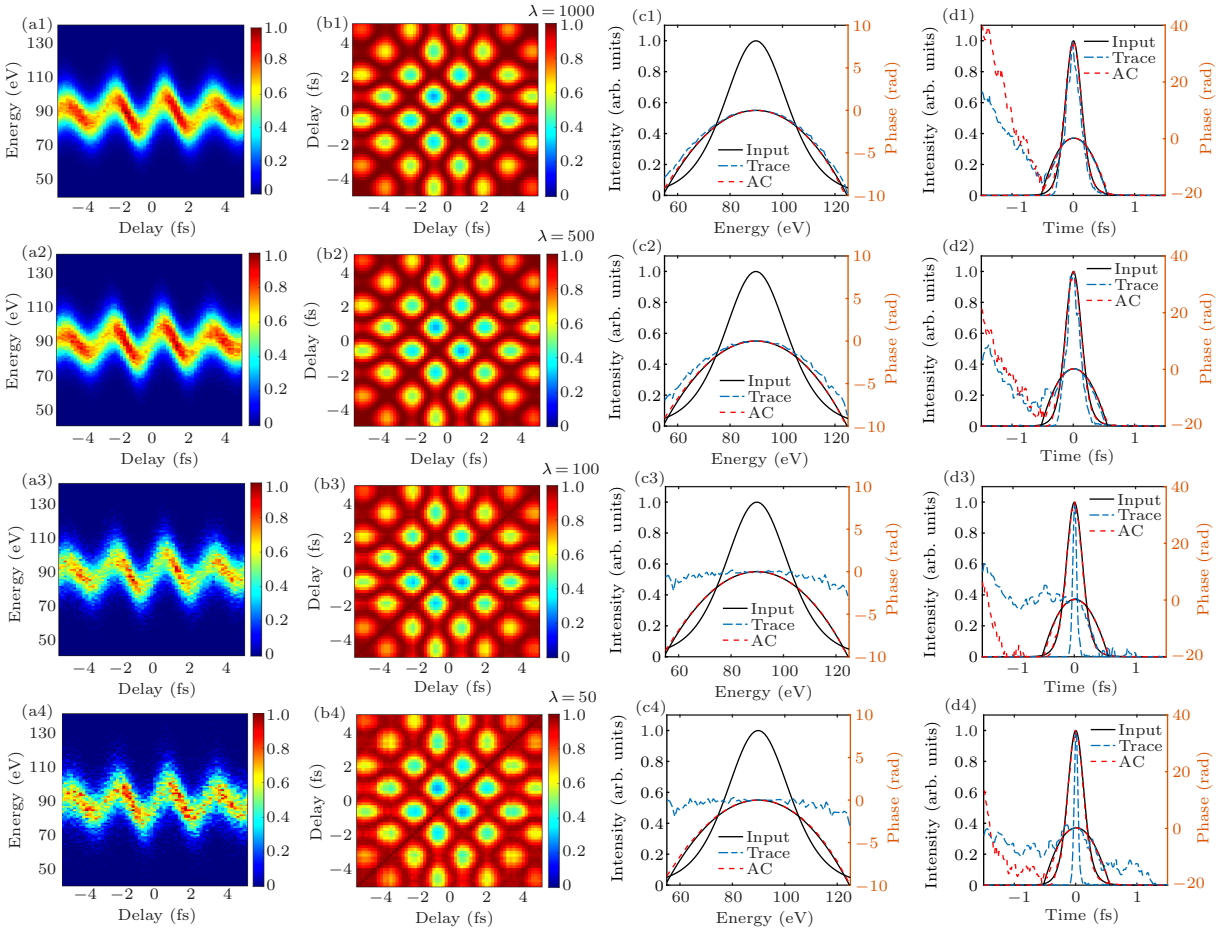


Fig. 4. Phase retrieval results using streaking traces (a1)–(a4) and autocorrelation traces (b1)–(b4). The test set includes Poisson noise with $\lambda_p = 1000$, 500, 100, and 50. Panels (c1)–(c4) compare retrieved and true spectral phases; panels (d1)–(d4) show the corresponding temporal phases and pulses.

Our results demonstrate that using autocorrelation traces as input to CNN models significantly enhances the accuracy and robustness of attosecond pulse characterization, particularly under realistic noise conditions. This approach offers a promising direction for improving phase retrieval in experimental settings where noise is unavoidable.

To benchmark the performance of our autocorrelation model, we compare it with several established retrieval algorithms, including PCGPA,[10] LSGPA,[11] PROOF,[12] ePIE[13] and VTGPA.[14] As illustrated in Fig. 5, the streaking trace from the attosecond streak camera used for the retrieval is shown in Fig. 5(a), serving as the input data for all iterative methods. The corresponding autocorrelation traces shown in Fig. 5(b), derived from the simulated streaking trace, serve as the input data for the autocorrelation (AC) model. The results in Fig. 5(c) compare the spectral phase retrieved

by each algorithm, indicating that while all methods capture the phase variation near the pulse center reliably, our model achieves higher accuracy across the spectrum. Furthermore, figure 5(d) presents the time-domain phase and pulse width results, demonstrating that our approach reconstructs the pulse profile more accurately. The temporal pulse widths retrieved by each method (in attoseconds) are as follows: input: 76.0, AC: 75.0, PCGPA: 75.0, LSGPA: 76.0, PROOF: 79.0, ePIE: 76.0, and VTGPA:73.0. These results highlight the superior precision of our approach, particularly in comparison to other methods that show significant deviations from the expected temporal width. More importantly, the CNN-based model offers a remarkable advantage in computational speed. Once trained, the model delivers retrieval results almost instantaneously, a capability that traditional iterative algorithms cannot match. This rapid processing makes the CNN-based approach especially valuable for large-scale data analysis, where efficiency and speed are critical. Its practical utility is further demonstrated by the ability to process complex datasets with minimal delay, enhancing its suitability for real-time applications. Thus, the CNN-based method proves to be not only accurate but also highly efficient, making it a robust and effective tool for pulse retrieval.

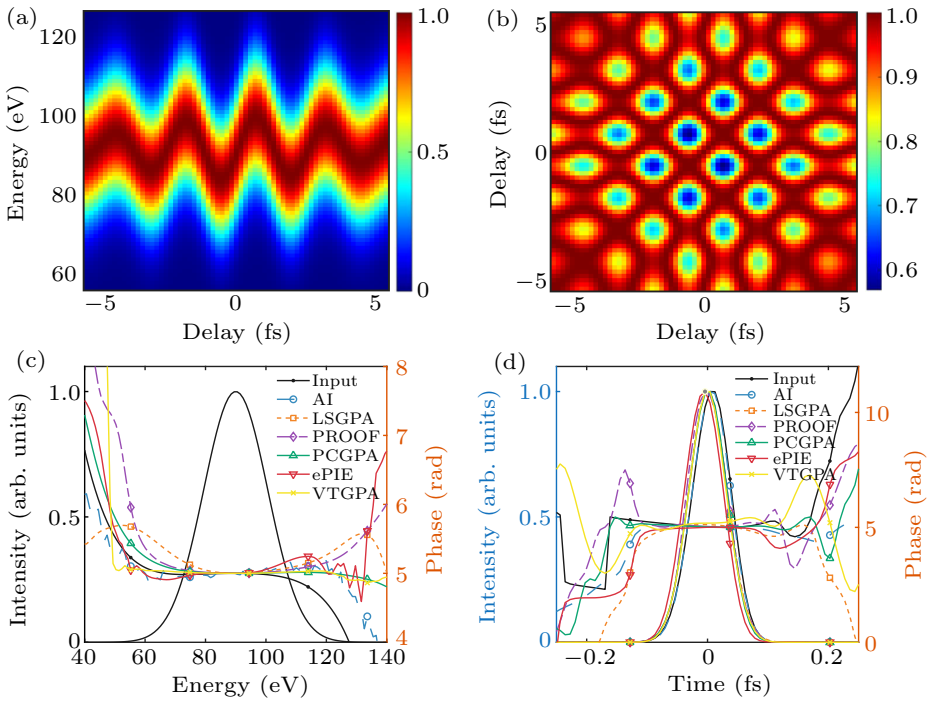


Fig. 5. Comparisons of results from different retrieval algorithms. (a) The simulated streaking trace from the attosecond streak camera used as the retrieval target. (b) The corresponding autocorrelation traces derived from the simulated streaking trace. (c) Comparisons of the spectral phases retrieved by different algorithms. (d) Comparisons of the time-domain phases and reconstructed pulse profiles obtained using different retrieval algorithms.

In summary, the autocorrelation-based CNN model demonstrates superior robustness and accuracy, particularly with noisy datasets, compared to conventional retrieval methods. The inversion results show that while our model achieves similar predictive accuracy as mainstream techniques, it does so with a significant advantage in computational speed. The model's robustness in practice ensures both reliability and efficiency, offering an ideal solution for pulse retrieval tasks. Future work will focus on refining the model to further improve its performance and extending its applications to a wider range of domains. This study provides valuable insights into the potential of CNN-based models for advancing phase retrieval algorithms, particularly for attosecond pulses and diffraction imaging.

Acknowledgements

Project supported by the CAS project for Young Scientists in Basic Research (Grant Nos. YSBR-059 and YSBR-115) and the National Natural Science Foundation of China (Grant No. 92150103).

References

[1] Krausz F and Ivanov M 2009 *Rev. Mod. Phys.* **81** 163

[2] Goulielmakis E, Loh Z H, Wirth A, Santra R, Rohringer N, Yakovlev V S, Zherebtsov S, Pfeifer T, Azzeer A M, Kling M F, Leone S R and Krausz F 2010 *Nature* **466** 739

[3] Ott C, Kaldun A, Argenti L, Raith P, Meyer K, Laux M, Zhang Y, Blättermann A, Hagstotz S, Ding T, Heck R, Madroñero J, Martín F and Pfeifer T 2014 *Nature* **516** 374

[4] Schultze M, Ramasesha K, Pemmaraju C D, Sato S A, Whitmore D, Gandman A, Prell J S, Borja L J, Prendergast D, Yabana K, Neumark D M and Leone S R 2014 *Science* **346** 1348

[5] Calegari F, Ayuso D, Trabattoni A, Belshaw L, De Camillis S, Anumula S, Frassetto F, Poletto L, Palacios A, Decleva P, Greenwood J B, Martín F and Nisoli M 2014 *Science* **346** 336

[6] Ghimire S, Ndabashimiye G, DiChiara A D, Sistrunk E, Stockman M I, Agostini P, DiMauro L F and Reis D A 2014 *J. Phys. B: At. Mol. Opt. Phys.* **47** 204030

[7] Hentschel M, Kienberger R, Spielmann C, Reider G A, Milosevic N, Brabec T, Corkum P, Heinzmann U, Drescher M and Krausz F 2001 *Nature* **414** 509

[8] Gaumnitz T, Jain A, Pertot Y, Huppert M, Jordan I, Ardana-Lamas F and Wörner H J 2017 *Opt. Express* **25** 27506

[9] Mairesse Y and Quéré F 2005 *Phys. Rev. A* **71** 11401

[10] Kane D J 2008 *J. Opt. Soc. Am. B* **25** A120

[11] Gagnon J, Goulielmakis E and Yakovlev V S 2008 *Appl. Phys. B* **92** 25

[12] Chini M, Gilbertson S, Khan S D and Chang Z 2010 *Opt. Express* **18** 13006

[13] Lucchini M, Brügmann M H, Ludwig A, Gallmann L, Keller U and Feurer T 2015 *Opt. Express* **23** 29502

[14] Keathley P D, Bhardwaj S, Moses J, Laurent G and Kärtner F X 2016 *New J. Phys.* **18** 73009

[15] Yu W W, Zhao X, Wei H, Wang S J and Lin C D 2019 *Phys. Rev. A* **99** 33403

[16] Fukushima K 1980 *Biol. Cybern.* **36** 193

[17] LeCun Y, Bengio Y and Hinton G 2015 *Nature* **521** 436

[18] Genty G, Salmela L, Dudley J M, Brunner D, Kokhanovskiy A, Kobtsev S and Turitsyn S K 2021 *Nat. Photon.* **15** 91

[19] White J and Chang Z 2019 *Opt. Express* **27** 4799

[20] Zhu Z, White J, Chang Z and Pang S 2020 *Sci. Rep.* **10** 5782

[21] Brunner C, Duensing A, Schröder C, Mittermair M, Golkov V, Pollanka M, Cremers D and Kienberger R 2022 *Opt. Express* **30** 15669

[22] Singh P and Manure A 2020 *Learn Tensorflow* 2.0 (Berkeley, CA: Apress) p. 1

[23] Kitzler M, Milosevic N, Scrinzi A, Krausz F and Brabec T 2002 *Phys. Rev. Lett.* **88** 173904

[24] Lewenstein M, Balcou Ph, Ivanov M Yu, L'Huillier A and Corkum P B 1994 *Phys. Rev. A* **49** 2117

[25] Itatani J, Quéré F, Yudin G L, Ivanov M Yu, Krausz F and Corkum P B 2002 *Phys. Rev. Lett.* **88** 173903

[26] Asuero A G, Sayago A and González A G 2006 *Crit. Rev. Anal. Chem.* **36** 41

[27] Zhang Z 2018 *IEEE/ACM International Symposium on Quality of Service* (26th.) (Banff, AB, Canada) p. 1